Modeling Scale Formation in Flat-Sheet Membrane Modules During Water Desalination

Margaritis Kostoglou
Div. of Chemical Technology, Dept. of Chemistry, Aristotle University, Thessaloniki 541 24, Greece

Anastasios J. Karabelas
Chemical Process and Energy Resources Institute, Centre for Research and Technology—Hellas, Thermi, Thessaloniki, 570 01, Greece

DOI 10.1002/aic.14045
Published online February 22, 2013 in Wiley Online Library (wileyonlinelibrary.com)

Modeling the operation of spiral-wound membrane modules is essential for their successful design and optimization. Such models must include the main types of membrane fouling, degrading desalination plant performance, including scaling due to sparingly soluble salts. Unfortunately, the complexity of underlying physicochemical processes and the coexistence of several spatial and temporal scales render intractable modeling of membrane scaling based on first principles. Therefore, a suitable (albeit simplified) framework is developed for incorporating scaling dynamics into a fluid flow model formulated at an intermediate (i.e., mesoscopic) length scale of membrane operation. The general mesoscopic approach involves integration of spatially distributed submodels, thereby allowing predictions at the large (entire membrane sheet) scale; these submodels comprise constitutive laws and kinetic rate expressions derived at fine scales. A submodel for the effect of pre-existing bulk particles on scale formation is developed herein. Several numerical results are presented to exemplify the potential of the proposed framework. © 2013 American Institute of Chemical Engineers *AIChE J*, 59: 2917–2927, 2013

Keywords: membrane modules, desalination, mathematical modeling, scaling

Introduction

The use of reverse osmosis (RO) membranes for water treatment has rapidly expanded during the last two decades.[1] Among several designs of reverse osmosis membrane elements, the so-called spiral-wound module (SWM), comprised membrane sheets and spacers in-between, seems to offer an overall optimum balance between operational requirements, fouling control, efficiency, and packing density.[2] SWM is widely used for several types of applications characterized according to the operating pressure; for example, for high-pressure sea-water desalination, low-pressure brackish water desalination, ultra-low-pressure water, or waste-water purification.

Membrane fouling is considered as the main problem that causes degradation of SWM performance, negatively affecting energy consumption, permeate quality, and overall process efficiency. The development of a fouling layer on membrane sheets is determined by the locally varying flow field parameters, including trans-membrane pressure, fluid permeation flux, and cross-flow velocity at the retentate side; therefore, fouling is characterized by spatial nonuniformity throughout the membrane sheets of each element. To improve SWM element design and operation, adequate knowledge (not available at present) is necessary on the temporal and spatial variation of the above parameters across pressure vessels. The great difficulties in tackling this problem are well known, as several types of membrane fouling can occur (often simultaneously) in practical water treatment operations; that is, scaling due to sparingly soluble salts,[3] organic gel-layer formation,[4] biofouling,[5] and colloidal particle deposition.[6] In general, the effect of deposits is to reduce the effective permeabilities of both the membrane and the narrow retentate channels, with obvious negative consequences. The relative significance of this effect on channel and membrane permeability depends on the type and extent of fouling, which is at present extremely difficult to predict as a function of feed-water properties and process conditions.

The development of reliable mathematical models to describe the performance of SWM is essential for the individual module design and optimization as well as for the design and performance assessment of an entire plant. Consequently, the literature on SWM modeling is significant, extending from simple empirical models to multiscale models based on "communicating information" between length scales to overcome the inherent complexity of the process. A few modeling works dealing with SWMs include fouling. Moreover, the mode of fouling seldom incorporated in mathematical models is scaling. The strong nonlinearity of this problem with respect to the locally prevailing conditions on the membrane is invoked as source of uncertainty[7] discouraging researchers; thus, typically the consideration of scaling is restricted to the estimation of local supersaturation.[7]

Correspondence concerning this article should be addressed to M. Kostoglou at kostoglu@chem.auth.gr.

Recently, a model of scaling during dead-end membrane desalination was developed[8,9] based on crystallization/precipitation theories, also incorporating population balances. The basic features of that model are transferred here to the much more complicated geometry of SWM. This work is considered a step toward the development of a generalized SWM model that should account for all aspects of their operation, including fouling. In the following, a general assessment of the modeling requirements for the SWM operation is made first, and the sequence of simplifications/assumptions that leads from the actual problem complexity to a feasible model is presented. Next, a particular approach is presented for incorporating the scaling process submodel into the entire-membrane scale (i.e., the "large-scale") modeling framework. An approach to account for the (commonly observed in practice) pre-existing particles in the feed-fluid is also presented. Finally, several results focused on the innovative aspects of the present model are presented and discussed.

Problem Formulation

The complete problem of simulating the physical phenomena occurring during operation of a RO membrane module is extremely complicated; thus, a simplification path must be followed. The physical problem considered here refers to a flat-sheet membrane; that is, curvature of SWM is ignored. Very few studies have investigated the impact of the SWM geometry on module performance, including that of membrane curvature that might influence the large-scale flow. As the focus here is on scaling phenomena at small length scale, neglecting curvature is considered reasonable at this stage of model development. A further simplification allowing reduction in the dimensionality of the macroscopic problem is that the pressure drop in the permeate side is insignificant (or practically zero in specially designed small-size modules for experimental study). Hence, the process modeled here is restricted to the retentate side of the membrane. This approximation is very familiar in the literature for models of RO membrane operation,[10] but it can be removed in future model development.

This work is focused on the "evolution" of scale on the membrane due to the supersaturation of sparingly soluble salts. The possibility is also considered that a small amount of colloidal particles of such salts is contained in the feed flow. To be sure, this is not an attempt to study particulate or colloidal fouling; however, one must take into account the small amount of particles, commonly present in feed-waters in practice, which influence the scaling process. The difference of this work, compared to many literature studies on the subject, is the inclusion of the scaling process in the modeling framework for the entire membrane sheet.

The problem to be solved will be described without explicitly presenting the governing equations. These equations have only formalistic interest, and they are not amenable to solution before a significant degree of simplifications/approximations is achieved. The complications in formulating the problem, for spacer-filled channels, are due to several sources: the first is due to the geometry, as there are three length scales of interest in the mathematical problem; that is, the size scale of surface-particles, the spacer filament size scale, and the macroscopic (membrane sheet) size scale. A second source of complexity is the flow unsteadiness.[11,12] There are two main time scales related to unsteadiness: the first is associated with the scale growth and the second (a finer one) is inherent in the fluid dynamics of the process. Indeed, the fluid flow in the geometry created by the spacers and for Reynolds numbers of practical interest is unsteady leading to a chaotic flow pattern.[11,12] Another source of difficulty is the complex chemistry of the salts of practical interest. These salts are not dissociated directly but through several intermediates; however, typically, supersaturation is computed using chemical equilibria codes assuming spatially homogeneous conditions.[13] Moreover, interactions between the salts make the situation even worse.[14] Finally, modeling the formation of the solid phase during the precipitation of the salts induced by local supersaturation, both in the fluid bulk and on the membrane surface, is always a demanding task.

The direct way to attack the problem is to use the fluid dynamics equations, the mass conservation equations for all the participating molecular and ionic species, the population balance equations for the bulk particles, and the discrete particle nucleation and growth equations for the surface particles. The mass conservation equations must include chemical reaction terms, as the governing reactions may be shifted from equilibrium.[15] Phenomena associated with ion transport must be also considered in these equations. A direct attack for solving the above problem is out of the question, so the following simplification procedures are used.

The spacer-scale problem is generally solved by using computational fluid dynamics (CFD) approaches, considering only the fluid dynamics and the mass conservation equations of a single species (i.e., ignoring the ionic structure of the scaling compounds). Among several reported approaches, regarding geometric representation and flow description,[16–18] the unit cell approach[19] is considered as the most appropriate in terms of accuracy and efficiency. In this approach, using advanced numerical techniques,[19] an exact solution of the conservation equations is obtained for a periodic unit cell and constitutive laws are extracted, applicable throughout the membrane.[20]

The direct incorporation of the actual chemistry in the complex flow field requires to account for the time scales of flow, diffusion, and reaction. This is one of the major problems in chemical engineering, which has not been solved yet for a combination of complicated flows and complex reaction schemes. There are some techniques for simplification of fast (compared to transport time scale) reactions,[21] even for bulk precipitation of $CaCO_3$, but they involve simple transport mechanisms (i.e., mainly diffusion[22]). The only attempt known, incorporating detailed chemistry to a surface precipitation model, has been recently made for the problem of $CaCO_3$ scaling in turbulent pipe flow, using a simple model for the scale growth.[23] Such a chemical scheme cannot be incorporated in the detailed CFD simulation; thus, the usual approach is to write down "apparent" conservation equations for major species and to assume chemical equilibrium locally at the position where supersaturation data are needed for the computation of precipitation rate.[8]

An even simpler approach used in purely theoretical studies is to consider the conservation of one species and to assume a single value of its solubility, defining the supersaturation as the ratio of the local concentration values and the solubility. This approach will be followed in this work targeting to model development and analysis. Combination of the present models with comprehensive chemical equilibria codes is straightforward and will be used in the future to

analyze experimental data. Even simplifying chemistry, the concentration field arising throughout the membrane sheet is too complex; thus, in a way similar to the hydrodynamics,[19] the multiscale approach is followed. The main requirement from the mass conservation equations is the knowledge of the concentration, at a depth near the membrane surface, which determines the osmotic pressure and the local wall flux. The flux-concentration interdependence leads to a two-way coupling between mass transfer and hydrodynamic problems. This coupling is typically ignored in the CFD simulations of the concentration fields for the spacer scale geometry, where either the wall flux is ignored[24] or a prescribed value is assumed.[18] The wall velocity creates a thin concentration boundary layer at the membrane surface and, thus, introducing another size scale in the problem.

Typically, the resulting concentration fields are used for the derivation of a time and space averaged Sherwood number, which is used by the macroscopic model. In general, the Sherwood number is shown to be a power law function of the Reynolds and Schmidt numbers; the exponents for the two numbers are different but in some cases equal exponents are assumed.[18] The Sherwood number is used for the estimation of the concentration polarization modulus that relates the bulk and surface concentration in the channel through the so-called film theory.[25] The majority of the computational and theoretical work on the concentration polarization and its approximation with the film theory or similar techniques refers to steady laminar flows in which *Sh* varies along the flow.[26] However, in highly dispersive flows like the present one, *Sh* does not change along the flow leading to a constant concentration polarization modulus. Here, the *Sh* number relations based on three-dimensional (3-D) unit cell CFD simulations[24] are used; it is noted that permeate flow is ignored in these simulations. It is well known from old theoretical works on heat transfer[27] and from recent numerical simulations of concentration polarization[7] that the *Sh* number is linearly related to the wall Peclet number (i.e., Peclet number based on wall velocity). This contribution may be substantial for laminar flow where transverse transport is dominated by conduction, but it is certainly insignificant for flows with high degree of mixing where transverse transport also occurs by convection.

An additional source of complexity is related to the surface precipitation process, described by nucleation and particle growth steps for discrete particles. There are two levels of averaging required to go from the discrete particle scale to the mesoscopic (membrane sheet) scale: the first is related to homogenization with respect to particle scale and the second to the homogenization in the unit cell. Unit cell homogenization has been theoretically justified for hydrodynamics (considering a moderately nonlinear process) in narrow channels with spacers.[20] However, the expected accuracy of the homogenization for highly nonlinear processes such as precipitation is questionable. Fortunately, recent experimental results from this laboratory[28] suggest that the surface particle concentration and size essentially do not vary throughout a unit cell of the spacer pattern.

The preceding critical assessment, starting from first principles, has resulted in a set of physical assumptions on which the model of the scaling process is based. It is noted that the model presented herein considers complete rejection of salts by the membrane, which is quite realistic for RO desalination processes; however, its extension to arbitrary rejection (that may apply to other desalination processes such as nanofiltration) is straightforward. The basic aspects of the model will be presented separately as follows. It is stressed here that addressing the entire membrane operation is extremely complicated, and there are two general approaches to proceed in modeling tasks. The first is to develop empirical models and to extract parameters using data from real membrane operations; the second and more ambitious one is to develop locally applicable models, based on first principles, and to extract physical parameters from model experiments that isolate or eliminate particular aspects of the practical process, for example, by dealing with a single fouling mode or by eliminating flow field complexities. This work deals with the model-development part of the second approach. In parallel, experiments have already been performed, without the flow field complexity created by the spacer, to extract realistic precipitation parameter values[8]; furthermore, membrane scaling experiments, performed in spacer-filled narrow channels (simulating local conditions in flat-sheet membrane modules), provide detailed data of incipient scale formation,[28] helpful in this direction.

Scale development

The presentation starts from the scale development equations. The driving force for surface precipitation is the existence of supersaturation; that is, local salt concentration corresponding to a supersaturation ratio larger than unity. The precipitation proceeds by two mechanisms, that is, nucleation that creates new surface particles and particle growth that leads to size increase of the previously created particles. The particle shape is assumed to be a hemisphere (i.e., contact angle with the substrate $\pi/2$) without lack of generality, as the shape effect can be absorbed into the kinetic parameters. According to nucleation theory,[29] the nuclei diameter d_c (m) is given as

$$d_c = \frac{4V_m\sigma_{het}}{k_B T \ln(S)} \tag{1}$$

where V_m (m^3) is the molecule volume of the solid phase, σ_{het} (N/m) the surface energy for heterogeneous nucleation, T the temperature (K), and k_B the Boltzmann constant [$m^2kg/(s^2$ K)]. The volume of the hemispherical nuclei is $\alpha_c = (\pi d_c^3)/12$. The surface nucleation rate is given by the relation

$$J_n = A_n \exp\left(-\frac{16\pi\sigma_{het}^3 V_m^2}{3(k_B T)^3 (\ln(S))^2}\right) \tag{2}$$

The units of J_n are number of nuclei per square meter per second (#/m^2/s). The pre-exponential coefficient A_n (#/m^2/s) can vary by several orders of magnitude, and the only way to be determined (like σ_{het}) is by fitting model results to experimental data for the particular system under study. The following parameter is used for clarity of presentation

$$B_n = \frac{16\pi\sigma_{het}^3 V_m^2}{3(k_B T)^3} \tag{3}$$

In general, the particle grows through two sequential steps, that is, diffusion of the active substances from liquid to particle surface and surface reaction on the particles. For the small particle sizes of interest in the present application, the diffusion step is very fast and can be neglected. The surface reaction rate expression considered here corresponds to a polynuclear growth mechanism. This mechanism implies layer by layer growth with multiple two-dimensional nuclei

in each layer. The molar rate of produced solid salt per unit area is given as[30]

$$J_R = k_R S^{7/6}(S-1)^{2/3}(\ln(S))^{1/6} e^{-E_R/\ln(S)} \quad (4)$$

where the units of J_R are moles of the salt per square meter per second [mol/(m^2 s)], k_R is a rate constant having the same units as J_R, and E_R is a dimensionless parameter that defines the sensitivity of the growth rate to the supersaturation. Taking into account the assumption of hemispherical shape of particles, the molar flux rate can be transformed to the volumetric growth rate for a particle of volume x

$$G(x) = 3^{2/3}(2\pi)^{1/3}\frac{J_R}{V_m N_A}x^{2/3} \quad (5)$$

where N_A is the Avogadro number and the units of G are m^3/s. The probability density function of the surface concentration of particles with volume x (units number/m^3) is defined as $f(x,t)$. The evolution equation for f considering nucleation and growth phenomena is as follows

$$\frac{\partial f(x,t)}{\partial t} + \frac{\partial G(x) f(x,t)}{\partial x} = J_n \delta(x-\alpha_c) \quad (6)$$

The function δ is the well-known Dirac delta function, and it is used to designate the generation of new particles of size α_c. For the problem at hand, the knowledge of only some integral properties of the particle-size distribution is sufficient, so the monodispersed distribution approximation can be applied. The zero and first moments of $f(x,t)$ denote the particle number and deposit mass per surface area, respectively, and are defined as

$$M_i = \int_0^\infty x^i f(x,t)\,dx \quad i=0,1 \quad (7)$$

The units of M_o are #/m^2 and of M_1 are $m^3/m^2 = m$. Multiplication of Eq. 6 by x^i and integration of both sides, from $x=0$ to $x=\infty$, results in

$$\frac{\partial M_i}{\partial t} = -[G(x) f(x,t)]_0^\infty + i\int_0^\infty x^{i-1} G(x) f(x,t)\,dx = \alpha_c^i J_n \quad i=0,1 \quad (8)$$

Assuming a monodisperse form for the particle-size distribution, that is, $f(x,t) = M_o \delta(x - M_1/M_o)$ a closed problem results with respect to the moments M_o and M_1, which takes the form

$$\frac{dM_o}{dt} = A_n \exp\left(-\frac{B_n}{(\ln(S))^2}\right) \quad (9)$$

$$\frac{dM_1}{dt} = 3^{2/3}(2\pi)^{1/3} k_R V_m N_A S^{7/6}(S-1)^{2/3}(\ln(S))^{1/6} e^{-E_R/\ln(S)} M_o\left(\frac{M_1}{M_o}\right)^{2/3} + \alpha_c A_n \exp\left(-\frac{B_n}{(\ln(S))^2}\right) \quad (10)$$

It is noted that the above equations were derived for the case of small surface coverage by crystals (defined by scale coverage fraction φ). In some practical cases, the scale covers a large portion of the membrane surface and, thus, modifying its permeability; under such conditions, Eqs. 9 and 10 must be modified. The nucleation term in both equations must be multiplied by $(1-\varphi)$, because nuclei can be created only on the free from particles surface. For large surface coverage, overlapping between particles occurs, and modification of the growth term is also needed. The problem has been extensively discussed in the context of solid reaction theory[31] but much less for surface phenomena like the present one.[32] Nevertheless, the simulations reported here are restricted to $\varphi < 0.25$, which covers all cases of practical interest; therefore, it is realistic to ignore particle overlapping.

The concentration boundary condition for the CFD simulations must be a balance between convective flux, diffusive flux, and phase transformation rate, that is

$$v_w c + D\frac{\partial c}{\partial y} = \frac{1}{V_M N_A}\frac{dM_1}{dt} = R \quad (11)$$

where v_w (m/s) is the permeate wall velocity, D (m^2/s) the active substance diffusivity, and y the direction transverse to the main flow ($y=0$ on the membrane wall). In the following, the right-hand side term of Eq. 11 is denoted as R [mol/(m^2 s)] for clarity of presentation.

Membrane equations

The key question here is how to include the surface precipitation boundary condition to a description of the process at the membrane scale. In the absence of precipitation, the concentration in the wall region c_i is related to the bulk concentration c_m at the specific position along the membrane through the following film theory relation

$$c_i = c_m \exp\left(\frac{v_w}{k_m}\right)$$

where k_m is the mass-transfer coefficient. This equation can be derived by assuming a film close to the wall where transfer occurs only by diffusion, whereas outside the film perfect mixing occurs. A much more formal derivation of this expression is obtained by considering the total diffusivity function $D_T(y)$ comprised of molecular and turbulent diffusivity, dependent on the distance y from the wall.[33] Ignoring axial variation leads to the following equation holding at each location along the membrane

$$\frac{\partial}{\partial y}\left(vc + D_T(y)\frac{\partial c}{\partial y}\right) = 0 \quad (12)$$

where v is the liquid velocity toward the wall. The concentration boundary layer is restricted to a region close to the wall (thin film), so the assumption $v = v_w$ can be made. For the same reason, the far-field condition $c = c_m$ is transferred to $y \to \infty$. The wall boundary condition at $y=0$ is

$$v_w c + D\frac{\partial c}{\partial y} = R \quad (13)$$

The mass-transfer coefficient is related to $D_T(y)$ as $k_m = \left[\int_0^\infty \frac{1}{D_T(y)}\,dy\right]^{-1}$ (k_m units: m/s). Solving Eq. 12 with its boundary conditions, taking the value of c at $y=0$ and using the relation for mass-transfer coefficient leads to

$$c_i = c_m e^{v_w/k_m} + \frac{R}{v_w}\left(1 - e^{v_w/k_m}\right) \quad (14)$$

Thus, the problem is closed without an explicit knowledge of $D_T(y)$; only the coefficient k_m must be known. This

coefficient can be obtained in the form $Sh = \alpha Re^{\beta} Sc^{\gamma}$ from the unit cell CFD simulations.[24] In case of flow with high degree of mixing, the above approach is very accurate; indeed, under such conditions the flow consists of a core of uniform concentration c_m and a thin wall layer where concentration varies from c_m to c_i on the membrane surface, in a specified manner. The high values of $D_T(y)$ in the core and the small volumetric flow in the thin film (i.e., no inertia with respect to concentration variation) is the reason for the success of this approach.

Having modified the film theory to account for the surface precipitation, the basic equations for the membrane scale model are presented. From the 3-D unit cell CFD model simulations,[24] it was found that $\frac{\Delta p}{\Delta z} = -f_1 Re^{f_2}$.

This relation is transformed to the following equation for the pressure drop along the channel

$$\frac{\mathrm{dp}}{\mathrm{dz}} = -f_1 \frac{\rho^{1-f_2} \mu^{f_2}}{h^{1+f_2}} U^{2-f_2} \tag{15}$$

where p (N/m^2) is the pressure in the channel, z the direction along the channel, U the cross-sectional average velocity (m/s), ρ the liquid density (kg/m^3), and μ the liquid viscosity (kg/(m s)), h the half-height of the channel, and L the channel length. The liquid mass conservation leads to the relation

$$h \frac{\mathrm{dU}}{\mathrm{dz}} = -v_w \tag{16}$$

The mass conservation equation for the active substance (salt) takes the form

$$\mathrm{hU} \frac{dc_m}{\mathrm{dz}} = v_w c_m - R \tag{17}$$

The term R is added based on the fact that there is no mass accumulation in the film region, so the fluxes at its two boundary planes must be the same. The mathematical problem is completed through a relation between the wall velocity and the local pressure and membrane surface concentration c_i

$$v_w = \frac{k_w (1-\varphi)}{\delta \mu} (p - \Gamma c_i) \tag{18}$$

where k_w (m^2) is the membrane specific permeability, δ the membrane thickness, and Γ (N m/mol) the osmotic pressure coefficient. It is assumed that the permeance of the membrane is proportional to the fraction of its surface free of scale.[7] The system of equations must be solved for the operation in time, throughout the membrane sheet. The mass-transfer coefficient varies in time and space through its Re (and subsequently U) dependence. The boundary conditions are $c = c_o$ and $U = U_o$ at the inlet of the channel (feed conditions). In case of constant pressure operation, the inlet pressure is fixed (i.e., $p = p_o$ at $z = 0$). The problem is more complicated for the constant flux mode of operation where the inlet pressure is an unknown function of time $p_o(t)$ and must be determined from the (practically realistic) requirement of constant in time total permeate flow; that is

$$\int_0^L v_w \mathrm{dz} = \text{constant}$$

Effect of particles

The fate of the particles existing in the feed stream are of interest here. The study of the particle concentration field, in the presence of a permeable wall, has been extensively studied in the context of cross flow filtration[34] and colloidal fouling.[35] In the former case, the usual assumption is that the particles do not adhere on the porous wall, whereas in the latter particle–wall interactions may be considered. All the above studies deal with steady laminar flow. For unsteady flows, as in the present case, additional phenomena like turbulent diffusion and turbophoresis come into play.[36] Given that the problem dealt with here has not been studied before (i.e., the concentration of particles is very small, and there are particle–solute interactions), the following approach is taken, recognizing also that a direct attack is not possible. As in the case of the species concentration field, the particle field is composed of two regions; that is, the "core region" where the number concentration N (#/m^3) is uniform in the transverse direction (equal to N_m) and a "boundary layer" of greater particle concentration close to the permeable wall. The particle growth in the core region can be ignored because of the relatively low salt concentration and the small particle residence time therein (typically of the order of few seconds).

Assuming small particle size and concentration, transport mechanisms as lift force, shear induced diffusion, and turbophoresis can be ignored[37] leaving only convection toward the wall and turbulent diffusion as prevailing mechanisms. The governing equation is

$$\frac{\partial}{\partial \mathrm{y}} \left(\mathrm{vN} + D_{Tp}(y) \frac{\partial \mathrm{N}}{\partial \mathrm{y}} \right) = 0 \tag{19}$$

where $D_{Tp}(y)$ is the total diffusivity (molecular ant turbulent) of the particles. The boundary conditions are

$$\begin{aligned} &N = N_m \text{ at } y \to \infty \\ &v_w N + D_p \frac{\partial \mathrm{N}}{\partial \mathrm{y}} = r \text{ at } y = 0 \end{aligned} \tag{20}$$

where N_m is the particle concentration in the core of the flow. The quantity r (particles/(m^2 s)) is the rate at which particles are attached on the wall. In general, this quantity depends on the interaction forces (double layer and Van der Waals interaction) between particles and wall.[38] The analysis on the relation of r to these forces for nonporous wall can be found elsewhere.[39] The extension of the theory for porous walls is an open subject. A phenomenological approach is to assume r proportional to the convective flux of particles to the wall $r = \lambda v_w N_i$, where N_i is the concentration of the unattached particles at $y = 0$ and λ is a number between 0 and 1 denoting the probability of attachment and expected to depend on physical properties (surface potential and Hamaker constant) of the particles and the wall.

The above equations ignore the growth of particles, which is a realistic assumption. Indeed, the residence time of the boundary layer particles is greater than the corresponding time in the core, but still it is much smaller than the growth time scale of the surface particles; therefore, the increase of the dispersed particle size along the flow path can be ignored as a first approximation. Furthermore, the Sc number of the particles is much larger than the Sc number for the salt, so the particle boundary layer is much thinner than the salt boundary layer. In the scale of the salt concentration boundary layer, the particles appear to be located on a thin plane sheet adjacent to the wall, so the ionic species consumption for the growth of surface particles can be considered as a contribution to boundary condition (13) for the salt concentration equation. The surface concentration of the moving unattached particles can be found by integrating the particle

number concentration excess across the boundary layer. Solving Eq. 19 in a way similar to that of Eq. 12, results in

$$N=(N_m-\frac{r}{v_w})e^{\int_y^{\infty}\frac{1}{D_{Tp}(y\prime)}dy\prime}+\frac{r}{v_w} \tag{21}$$

Substituting the proposed expression for r and eliminating N_i leads to

$$N=N_m\left(\frac{1-\lambda}{1-\lambda+\lambda e^{v_w/k_m}}e^{\int_y^{\infty}\frac{1}{D_{Tp}(y\prime)}dy\prime}+\frac{\lambda e^{v_w/k_m}}{1-\lambda+\lambda e^{v_w/k_m}}\right) \tag{22}$$

Integrating the particle concentration excess across the boundary layer, the surface concentration N_s of the unattached particles is given as

$$N_s=N_m\left(\frac{1-\lambda}{1-\lambda+\lambda e^{v_w/k_m}}\right)\int_0^{\infty}\left(e^{\int_y^{\prime\infty}\frac{1}{D_{Tp}(y\prime\prime)}dy\prime\prime}-1\right)dy\prime \tag{23}$$

Having resolved approximately the particle concentration field, the particle effect can be incorporated in the developed membrane operation model. In particular, the attached particles contribute to the population of the surface particles, so the corresponding Eqs. 9 and 10 must be transformed to

$$\frac{dM_o}{dt}=A_n\exp\left(-\frac{B_n}{(\ln(S))^2}\right)+\lambda v_w N_m\frac{e^{v_w/k_m}}{1-\lambda+\lambda e^{v_w/k_m}} \tag{24}$$

$$\frac{dM_1}{dt}=3^{2/3}(2\pi)^{1/3}k_R V_m N_A S^{7/6}(S-1)^{2/3}(\ln(S))^{1/6}e^{-E_R/\ln(S)}M_o\left(\frac{M_1}{M_o}\right)^{2/3}+(1-\varphi)\alpha_c A_n\exp\left(-\frac{B_n}{(\ln(S))^2}\right)+\lambda v_w N_m\frac{e^{v_w/k_m}}{1-\lambda+\lambda e^{v_w/k_m}}\frac{\pi d^3}{6} \tag{25}$$

where d designates the average diameter of particles in the feed. The governing equation for N_m is derived in the same way as the equation for c_m; that is

$$hU\frac{dN_m}{dz}=v_w N_m-r=v_w N_m\frac{1-\lambda}{1-\lambda+\lambda e^{v_w/k_m}} \tag{26}$$

Finally, the boundary condition for the salt at $y=0$ (Eq. 13) is modified by adding a term of salt consumption by unattached particles. The solution of the salt conservation equations leads to the following modification of Eq. 14

$$c_i=c_m e^{v_w/k_m}+\frac{R}{v_w}(1-e^{v_w/k_m})+\frac{N_s\pi d^2 k_R S^{7/6}(S-1)^{2/3}(\ln(S))^{1/6}e^{-E_R/\ln(S)}}{v_w}\left(1-e^{v_w/k_m}\right) \tag{27}$$

The quantity R in the above equations corresponds to the one obtained from Eq. 10 and not from Eq. 25. To facilitate understanding, Figure 1 provides a schematic depicting particle involvement in the modeled membrane scaling process. The competition between surface and bulk particles for the membrane surface is also described schematically in a recent article,[40] but it is believed that the surface particle concentration is exaggerated there.

In case of particles, the complete profile $D_{Tp}(y)$ is needed instead of the mass-transfer coefficient. This can be determined by generalizing the form of the total diffusivity in turbulent pipe flow[41]; that is, $D_T=D+\frac{\mu}{\rho}q_1 Re^{q_2}\left(\frac{y}{h}\right)^{q_3}$.

The Sherwood number is related to D_T as follows

$$Sh=\frac{D}{h}\left[\int_0^{\infty}\frac{1}{D_T(y)}dy\right]^{-1} \tag{28}$$

Replacing the expression for D_T in the integral and matching the expression for Sh to the power law derived from unit cell CFD simulations,[24] the parameters q_i can be obtained for each type of spacers. For the small particles without inertia considered here, the turbulent diffusivity is just a flow property; thus, the total particle diffusivity can be determined from $D_{Tp}=D_p+\frac{\mu}{\rho}q_1 Re^{q_2}\left(\frac{y}{h}\right)^{q_3}$, where the Brownian particle diffusivity D_p is given by the Stokes–Einstein relation.

Indicative Results and Discussion

The model developed is rather complicated and includes many parameters and variables. Some additional complications can arise in practical cases of membrane operation. In many such cases, there are more than one salt in the liquid, so the above model should be extended accordingly. The salts in general behave in two different ways: in one limit, the highly soluble NaCl has a solubility, so large that its osmotic pressure inhibits membrane operation before precipitation occurs; in the other limit, the sparingly soluble salt (e.g., $CaCO_3$) is encountered in comparatively small concentration, leading to insignificant osmotic pressure increase but to significant scaling. However, there are salts of an intermediate behavior (i.e., exhibiting simultaneous precipitation and non-negligible osmotic pressure), usually in applications of desalting brackish water.[7] Nevertheless, in the case of desalting sea-water, the role of $CaCO_3$ and NaCl on the membrane operation and the way it is modeled can be different (however, directly accommodated in the general model presented here). In such a case, the model also allows to account for the well-known strong dependence of the $CaCO_3$ supersaturation on the local NaCl concentration.[14] Obviously, the real systems are so complicated that there is no meaning at this point to strive to obtain practical results, although they are, of course, the ultimate target of the model. Instead, results for specific aspects of the model (especially for the innovative ones) will be given, which will be also of relevance to special idealized experimental set-ups, and results to be obtained from them, for testing the theoretical modeling.

First, to focus on the surface precipitation model, a short membrane sheet is considered with an insignificant portion of the feed-fluid passing through the permeable wall. This is a typical laboratory experimental set-up, facilitating well-controlled parametric studies. In such a case, the variation of the variables along the short test-section is insignificant and can be totally ignored leading to a zero-dimensional model; that is, with time as the only independent variable. It is further considered that only one sparingly soluble salt exists, so

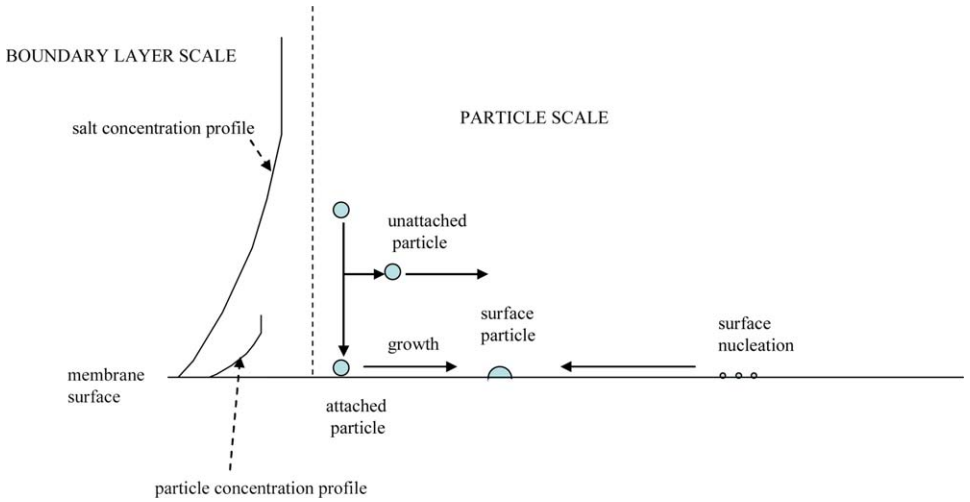

Figure 1. A schematic of the processes at particle and boundary layer scales.

Thick lines denote transfer by flow.

that the set of precipitation parameters used is very similar to those derived in a previous work by comparing theory and experimental results for membrane precipitation in a simpler dead-end filtration geometry.[8] A typical concentration for $CaCO_3$, encountered in practice, is used ($c_o = 2$ mol/m^3) and the following additional parameters are used for the sensitivity analysis: inlet supersaturation S_o, wall permeate velocity v_w, and mass-transfer coefficient k_m. Typical values for realistic conditions are assigned to these parameters, for the following cases: Case 1 ($S_o = 2$, $v_w = 3 \times 10^{-6}$ m/s, and $k_m = 10^{-5}$ m/s), Case 2 ($S_o = 2.5$, $v_w = 3 \times 10^{-6}$ m/s, $k_m = 10^{-5}$ m/s), Case 3 ($S_o = 2$, $v_w = 10^{-5}$ m/s, $k_m = 10^{-5}$ m/s), and Case 4 ($S_o = 2.5$, $v_w = 10^{-5}$ m/s, $k_m = 0.5 \times 10^{-5}$ m/s). Case 5 is also considered, which is the same as Case 3 but with the nucleation term not modified for the free surface area (using $1 - \varphi$); Case 5 is used to asses the effect of this correction. It is assumed that there are no particles in the feed stream. The set of scale formation model parameters used in all the examples is: $B_n = 25$, $\alpha_c = 10^{-26}$ m^3, $k_R = 5 \times 10^{-6}$ mol/(m^2 s), $E_R = 1$, and $V_m = 50 \times 10^{-6}$ m^3/mol.

In the following results, the time axis is in a logarithmic scale for convenience in the presentation of results. The simulations finish when the membrane surface fractional coverage φ exceeds 0.25 to obtain meaningful results. The evolution of the surface concentration is shown in Figure 2, for Cases 1–5. The initial values of the ratio c_i/c_m correspond to the concentration polarization modulus, which is much smaller in the presence of spacers compared to the unidirectional laminar flow case, that is, simple rectangular channel.[42] The modulus in general increases with increasing v_w and decreasing k_m. As the initial modulus increases and S_o increases, the precipitation rate increases leading to a faster reduction of the surface concentration c_i. Case 5 exhibits somewhat faster precipitation with respect to Case 3 as a result of neglecting the factor $1 - \varphi$ in the nucleation rate.

Figure 3 shows the evolution of the surface particle concentration for the cases considered. The particle number initially exhibits a rather steep increase, thereafter attaining a steady value when the salt concentration is reduced. Further scale development occurs only by growth of the existing particles. The evolution of the respective average surface particle diameter is shown in Figure 4.

In the case of relatively larger local supersaturation the number of nuclei is larger, so the size that can be attained by the particles is smaller, for a specified degree of surface coverage. The difference between Cases 3 and 5 is negligible, because it is related mainly to the particle number (nucleation). The evolution of the membrane surface coverage is shown in Figure 5. It is worth noticing the sensitivity of the scaling process to the basic problem parameters; that is, variation less than 100% of the quantities S_o, v_w and k_m leads to a range of characteristic times for scaling extending from 10 to 10^5 s.

The next step is to examine the effect of the particles present in the feed stream on the scale formation. The attached particles are simply added to the surface particles as is the case for the simpler geometry examined in a previous work.[9] The existence of unattached particles is an important aspect of this work, so the following results will be focused on them. Particle concentration profiles close to the membrane surface for several particle diameters are shown

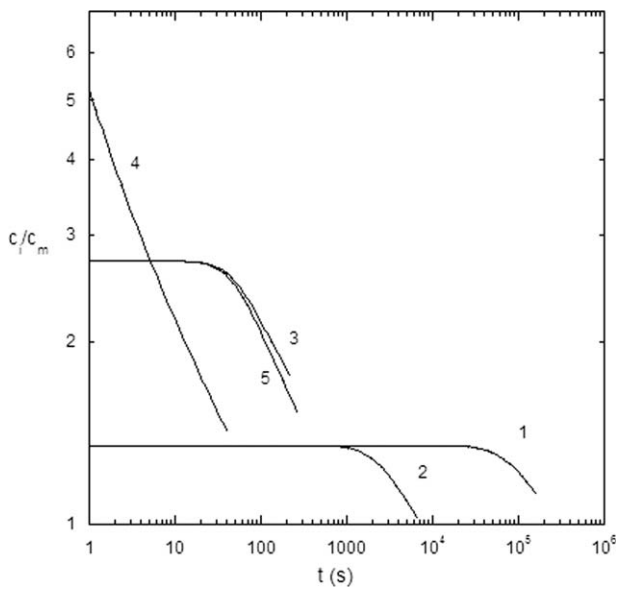

Figure 2. Evolution of the ratio c_i/c_m of surface to bulk salt concentration for Cases 1–5.

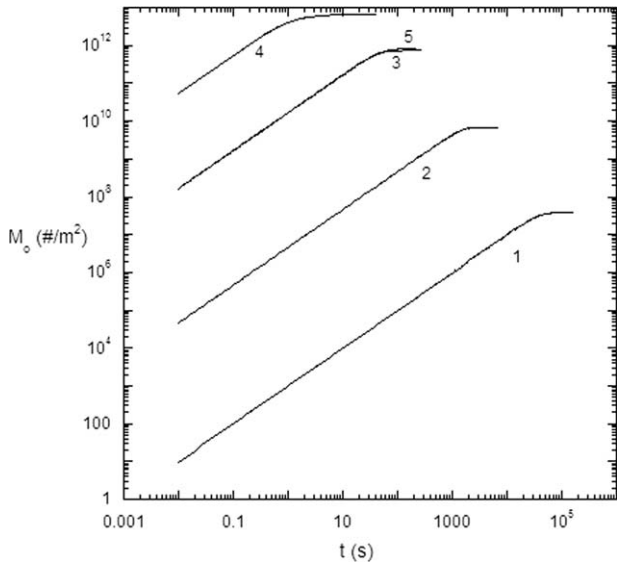

Figure 3. Evolution of surface particle number density M_o for Cases 1–5.

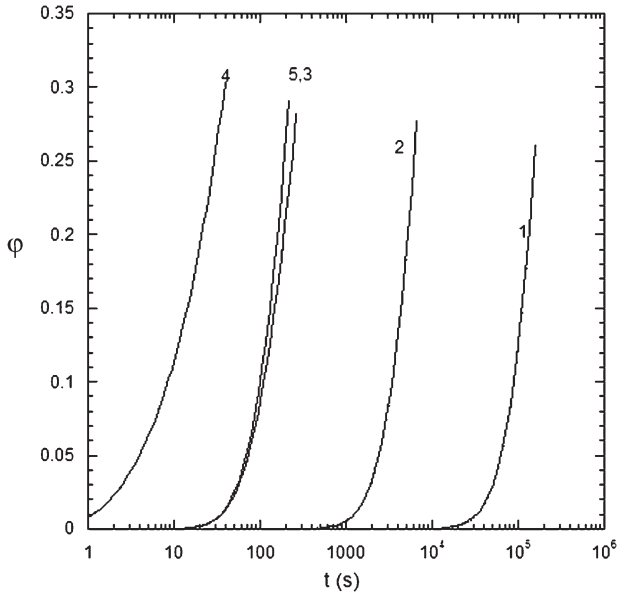

Figure 5. Evolution of fractional surface coverage by scale φ for Cases 1–5.

in Figure 6 (for $v_w = 3 \times 10^{-6}$ m/s, $Re = 100$, and $h = 0.5$ mm). As particle size increases, the particle diffusivity decreases leading to greater particle accumulation close to the surface. The thickness of the concentration boundary layer is of the order of 1 μm which means that for larger particles a scale breakdown occurs. Nevertheless, the assumption for the derivation of the present approach does not hold for larger particles. Taking into account the difficulties of considering discrete approaches for the bulk particles,[43] the present approach can be marginally used up to the limit of 1 μm for particle diameter. The particle accumulation decreases when attachment probability λ takes nonzero values. The normalized effective surface concentration of the unattached particles N_s/N_m vs. particle diameter is shown in Figure 7. The quantity N_s/N_m has inverse length units and is an increasing function of particle size and wall velocity. It is noted here that even a small value of probability λ can have a large effect on N_s for relatively large particles. To examine the effect of the particles on the scaling process, results from a specific case will be presented. The parameters of this case are ($k_m = 10^{-5}$ m/s, $v_w = 6$ μm/s, $d = 1$ μm, $S_o = 2$, and $\lambda = 0$). The concentration of the bulk particles in the feed stream is expressed through their volume fraction V_f in the dispersion, to render evident their small amount. Changing V_f from 10^{-12} to 10^{-10} the effect of particles varies from marginal to huge as can be seen from the c_i/c_m evolution

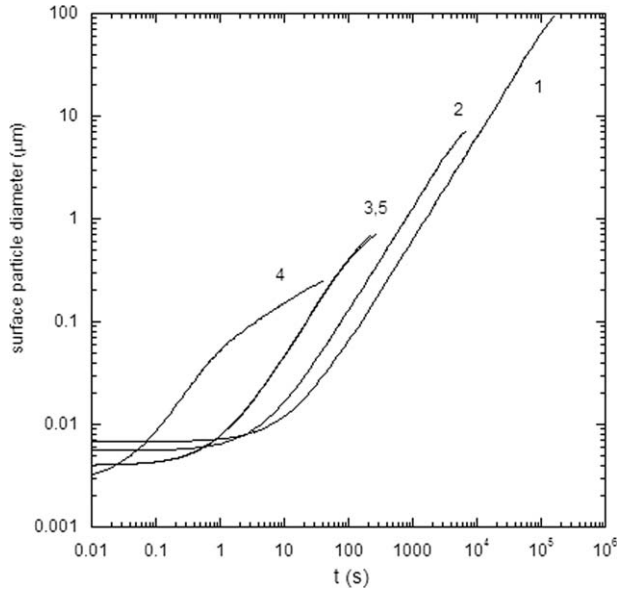

Figure 4. Evolution of average surface particle diameter for Cases 1–5.

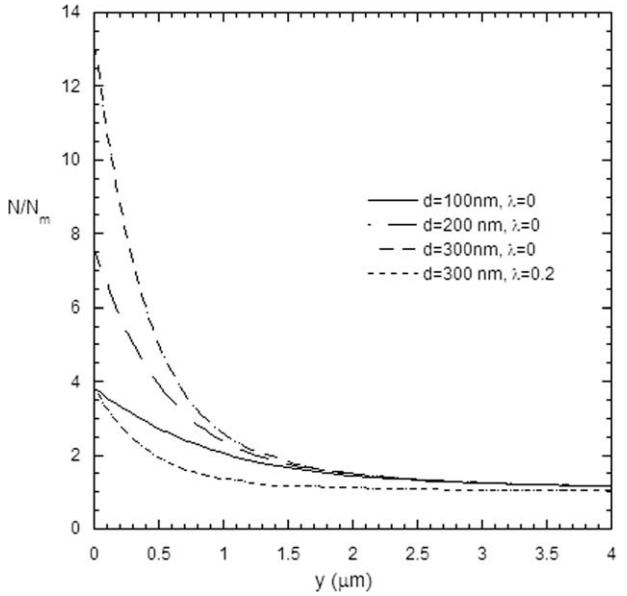

Figure 6. Normalized particle number concentration N/N_m vs. distance from the membrane surface for several particle diameters d and attachment probabilities λ.

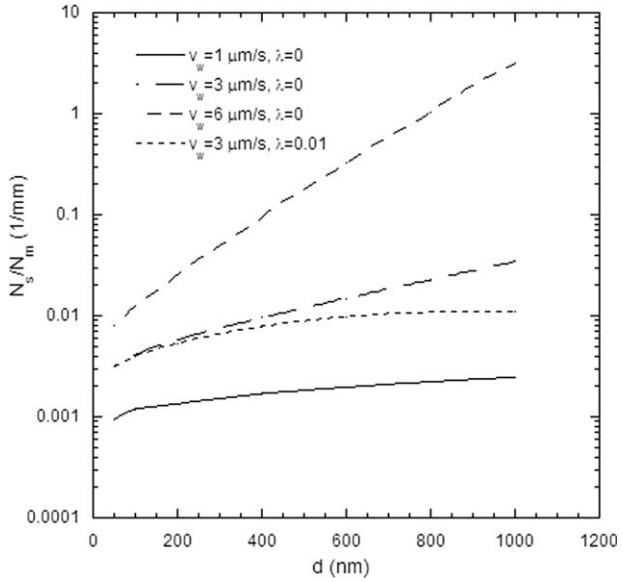

Figure 7. Ratio of effective surface concentration of unattached particles N_s to bulk particle concentration N_m vs. particle diameter d, for several wall velocities v_w, and attachment probabilities λ.

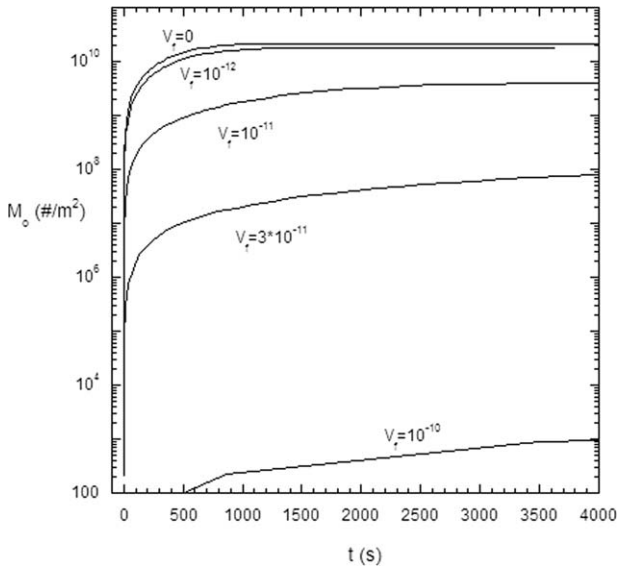

Figure 9. Evolution of surface particle number density M_o for several particle volume fractions V_f in the feed stream.

curves in Figure 8. Actually for $V_f = 10^{-10}$ all the salt amount, which is available for scaling, is consumed for growth of the unattached particles (exiting the membrane section considered) instead of being incorporated in the developing scale. The effect of the bulk particles on the evolution of the surface particles is presented in Figure 9. The number concentration of surface particles decreases, as V_f decreases and goes practically to zero for $V_f = 10^{-10}$. It is stressed that the case presented here is an extreme one with no particle attachment at all ($\lambda = 0$), but it clearly demonstrates the capabilities of the developed model to accommodate the physical phenomena involved.

A set of results regarding a sheet of realistic dimensions are presented next for the case of a sparingly soluble salt to demonstrate the capability of the model to describe the spatial evolution of scale. The prevailing conditions are $U_o = 0.1$ m, $v_w = 3 \times 10^{-6}$ m/s, $S_o = 2.5$, $L = 1$ m. The evolution of the spatial surface concentration profile (normalized with the inlet concentration c_o) is shown in Figure 10. Initially, the surface concentration increases along the channel due to increasing bulk concentration. With time, scaling on the membrane surface increases; therefore, the reacting species consumption rate for scale formation also increases. In general, the scale amount is greater toward the end of the channel due to the initial shape of the surface concentration profile. Furthermore, the increased scale mass at the end of the channel leads to a uniform concentration profile along the channel surface at intermediate stages. As the scaling process proceeds, the wall permeate velocity decreases due to reduced membrane permeation, which tends to reduce concentration polarization leading to the decreasing profile of c_i, shown in Figure 10 at long time values.

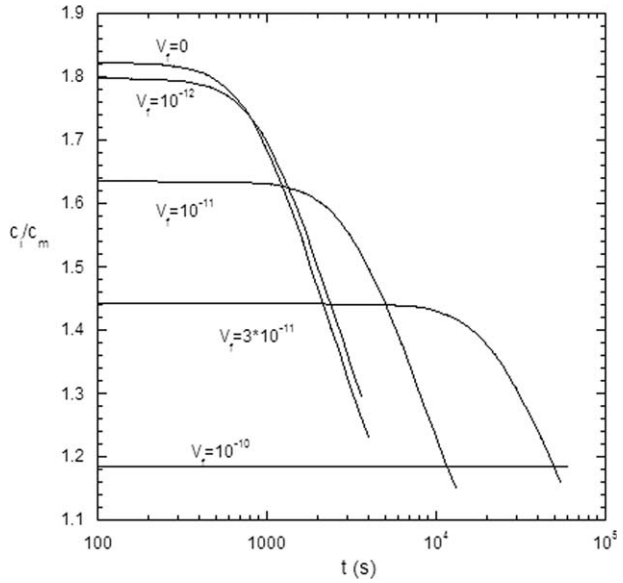

Figure 8. Evolution of the ratio c_i/c_m of surface to bulk salt concentration for several particle volume fractions V_f in the feed stream.

The evolution of the number density of the surface particles M_o along the channel is shown in Figure 11. The number density of particles tends to increase along the flow path. By comparing the profiles at times 2000 and 3000 s, it appears that the rate of formation of new particles decreases along the main flow direction. This is compatible with the reduction of the surfaces salt concentration along the flow discussed earlier. Figure 12 depicts the evolution of the axial profile of the average (over the size distribution) surface-particle diameter; the latter tends to monotonically decrease along the flow direction. This trend is attributed to the increasing number of particles along the main flow direction and to the surface concentration profile that tends to decrease along the flow as time proceeds. Finally, Figure 13 shows the temporal evolution of axial profiles of membrane surface coverage by scale. These profiles are monotonically increasing along the flow direction, in accord with the evolution of number density profiles. In the example of the sparingly soluble salt considered here, the osmotic pressure is assumed to be insignificant and for a high-pressure process the

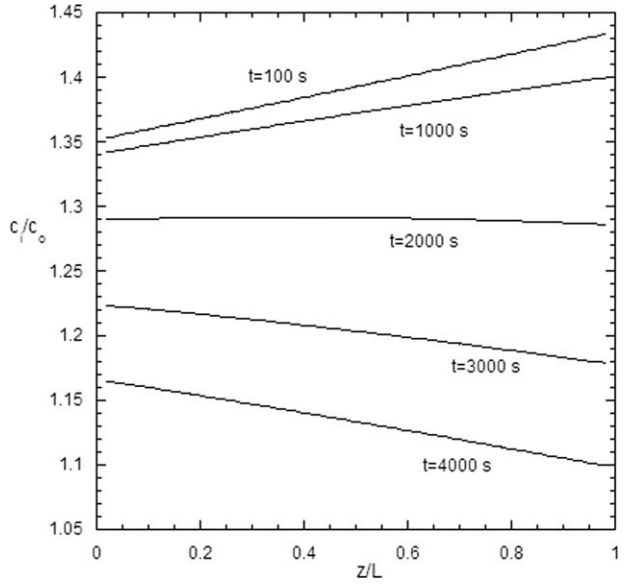

Figure 10. Profile of the ratio c_i/c_o (surface to inlet salt concentration) along the channel at several time values.

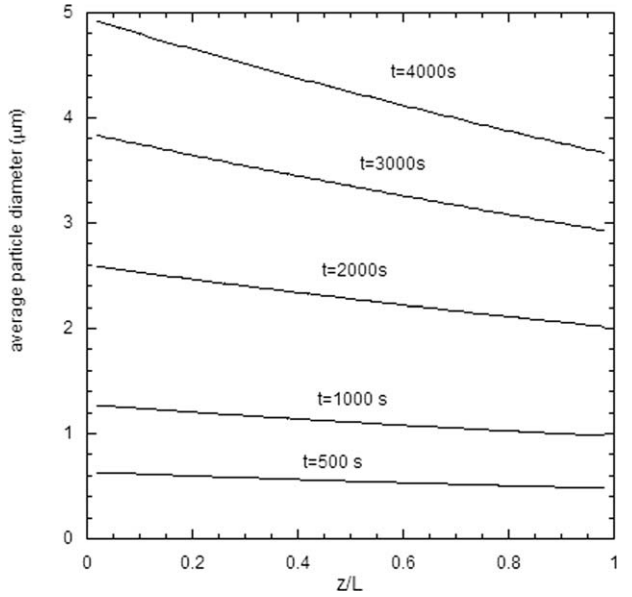

Figure 12. Profile of the average surface particle diameter along the channel at several time values.

profiles of the ratio v_w/v_{wo} are proportional to $1 - \varphi$. In summary, the typical results presented here, for isolated innovative aspects of the developed modeling framework, demonstrate how they can be integrated to simulate scaling evolution during an actual membrane operation.

Concluding Remarks

A general framework is presented for the development of a comprehensive modeling tool of SWM operation taking into account inorganic crystallization/scaling effects. The well-known approach of process scales separation is followed, whereby CFD simulations of transport phenomena in the spacer-filled channels of a module (at the unit cell level) are used to extract constitutive laws needed for the development of a global model applicable at the membrane-sheet scale. Starting from first principles, the line of assumptions and simplifications is presented in detail, which leads to engineering-type models without sacrificing the parameter dependence of phenomena involved. Special efforts are made to include the effect (on scaling) of particles usually existing in the feed stream to a membrane module. Future research activities involving the developed model will be along the following lines: first, it is planned to use the model for the assessment of detailed experimental data to be acquired in this laboratory, getting valuable insights that may lead to model adjustments and improvements. Second, this model will be integrated with other computational modules describing colloidal/organic fouling, into a general model aiming to simulate all aspects of practical SWM operation.

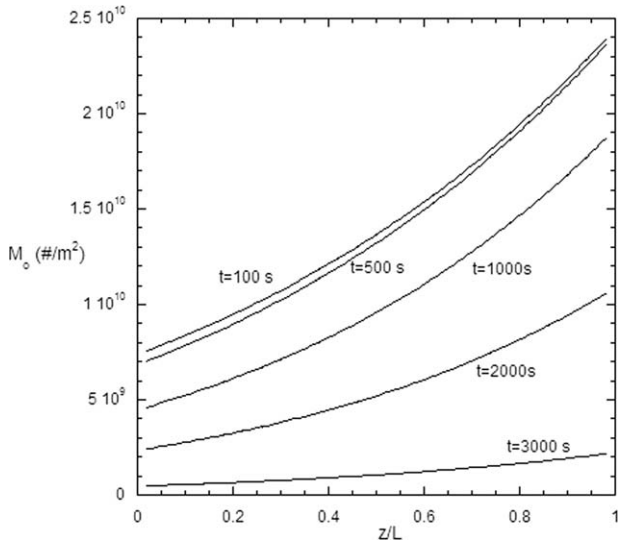

Figure 11. Profile of the surface particle number density M_o along the channel at several time values.

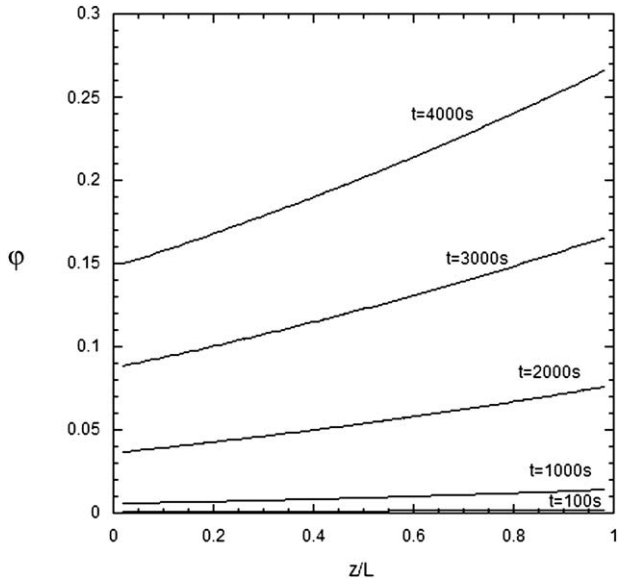

Figure 13. Profile of the surface coverage by scale φ along the channel at several time values.

Literature Cited

1. Membrane filtration in water treatment. In: Water Treatment: Principles and Design. New York: Wiley, 2005; Chapter 12.
2. Schwinge J, Neal PR, Wiley DE, Fletcher DF, Fane AG. Spiral wound modules and spacers. Review and analysis. *J Membr Sci*. 2004;242:129–153.
3. Hasson D, Drak A, Semiat R. Inception of $CaSO_4$ scaling on RO membranes at various water recovery levels. *Desalination*. 2001;139:73–81.
4. Schafer AI, Fane AG, Waite TD. Nanofiltration of natural organic matter: removal, fouling and the influence of multivalent ions. *Desalination*. 1998;118:109–122.
5. Vrouwenvelder JS, Graf von der Schulenburg DA, Kruithof JC, Johns ML, van Loosdrecht MCM. Biofouling of spiral-wound nanofiltration and reverse osmosis membranes: a feed spacer problem. *Water Res*. 2009;43:583–594.
6. Yiantsios SG, Sioutopoulos D, Karabelas AJ. Colloidal fouling of RO membranes: an overview of key issues and efforts to develop improved prediction techniques. *Desalination*. 2005;183:257–272.
7. Lyster E, Au J, Rallo R, Giralt F, Cohen Y. Coupled 3-D hydrodynamics and mass transfer analysis of mineral scaling-induced flux decline in a laboratory plate-and-frame reverse osmosis membrane module. *J Membr Sci*. 2009;339:39–48.
8. Karabelas AJ, Kostoglou M, Mitrouli ST. Incipient crystallization of sparingly soluble salts on membrane surfaces: the case of dead-end filtration with no agitation. *Desalination*. 2011;273:105–117.
9. Kostoglou M, Karabelas AJ. On modeling incipient crystallization of sparingly soluble salts in frontal membrane filtration. *J Colloid Interface Sci*. 2011;362:202–214.
10. Sundaramoorthy S, Srinivasan G, Murthy DVR. An analytical model for spiral wound reverse osmosis membrane modules: Part I. Model development and parameter estimation. *Desalination*. 2011;280:403–411.
11. Koutsou CP, Yiantsios SG, Karabelas AJ. Numerical simulation of the flow in a plane channel containing a periodic array of cylindrical turbulence promoters. *J Membr Sci*. 2004;231:81–90.
12. Fimbres-Weihs GA, Wiley DE. Review of 3D CFD modeling of flow and mass transfer in narrow spacer field channels in membrane modules. *Chem Eng Process*. 2010;49:759–781.
13. Sheikholeslami, R. Assessment of the scaling potential for sparingly soluble salts in RO and NF units. *Desalination*. 2004;167:247–256.
14. Schausberger P, Mustafa GM, Leslie G, Friedl A. Scaling prediction based on thermodynamic equilibrium calculation—scopes and limitations. *Desalination*. 2009;244:31–47.
15. Hasson D, Perl I. Scale deposition in a laminar falling-film system. *Desalination*. 1981;37:279–292.
16. Wardeh S, Morvan HP. CFD simulations of flow and concentration polarization in spacer filled channels for application to water desalination. *J Chem Eng Res Des*. 2008;86:1107–1116.
17. Wardeh S, Morvan HP. Detailed numerical simulations of flow mechanics and membrane performance in spacer-filled channels, flat and curved. *Desalination Water Treat*. 2009;1:277–288.
18. Guillen G, Hoek EMV. Modeling the impacts of feed spacer geometry on reverse osmosis and nanofiltration processes. *Chem Eng J*. 2009;149:221–231.
19. Koutsou CP, Yiantsios SG, Karabelas AJ. Direct numerical simulation of flow in spacer-filled channels: effect of spacer geometrical characteristics. *J Membr Sci*. 2007;291:53–69.
20. Kostoglou M, Karabelas AJ. On the fluid mechanics of spiral-wound membrane modules. *Ind Eng Chem Res*. 2009;48:10025–10036.
21. Okino MS, Mavrovouniotis ML. Simplification of mathematical models of chemical reaction systems. *Chem Rev*. 1998;98:391–408.
22. Gadhi KS, Kumar R, Ramkrishna D. Some basic aspects of reaction-engineering of precipitation processes. *Ind Eng Chem Res*. 1995;34:3223–3230.
23. Segev R, Hasson D, Semiat R. Rigorous modeling of the kinetics of calcium carbonate deposit formation. *AIChE J*. 2012;58:1222–1229.
24. Koutsou CP, Yiantsios SG, Karabelas AJ. A numerical and experimental study of mass transfer in spacer-filled channels: effects of spacer geometrical characteristics and Schmidt number. *J Membr Sci*. 2009;326:234–251.
25. Zydney AL. Stagnant film model for concentration polarization in membrane systems. *J Membr Sci*. 1997;130:275–281.
26. Kim S, Hoek EMV. Modeling concentration polarization in reverse osmosis processes. *Desalination*. 2005;186:111–128.
27. Raithby G. Laminar heat transfer in the thermal entrance region of circular tubes and two-dimensional rectangular ducts with wall suction and injection. *Int J Heat Mass Transfer*. 1971;14:223–243.
28. Mitrouli S, Karabelas AJ, Karanasiou A, Kostoglou M. Incipient calcium carbonate scaling of desalination membranes in narrow channels with spacers - experimental insights. *J Membr Sci*. 2013;425–426:48–57.
29. Sohnel O, Garside J. Precipitation: Basic Principles and Industrial Applications. Oxford: Butterworth-Heinemann, 1992.
30. Nielsen AE, Toft JM. Electrolyte crystal-growth kinetics. *J Cryst Growth*. 1984;67:278–288.
31. Khawam A, Flanagan DR. Solid-state kinetic models: basics and mathematical fundamentals. *J Phys Chem B*. 2006;35:17315–17328.
32. Kostoglou M, Andritsos N, Karabelas AJ. Incipient CdS thin film formation. *J Colloid Interface Sci*. 2003;263:177–189.
33. Sherwood TK, Brian PLT, Fisher RE, Dresner L. Salt concentration at phase boundaries in desalination by reverse osmosis. *Ind Eng Chem Fundam*. 1965;4:113–118.
34. Davis RH, Leighton DL. Shear induced transport of a particle layer along a porous wall. *Chem Eng Sci*. 1987;42:275–281.
35. Chen JC, Kim AS. Monte Carlo simulation of colloidal membrane filtration: principal issues for modeling. *Adv Colloid Interface Sci*. 2006;119:35–53.
36. Guha A. A generalized mass transfer law unifying various particle transport mechanisms in dilute dispersions. *Heat Mass Transf*. 2008;44:1289–1303.
37. Davis RH, Sherwood JD. A similarity solution for steady state cross flow microfiltration. *Chem Eng Sci*. 1990;45:3203–3209.
38. Russel WB, Saville DA, Schowalter WR. Colloidal Dispersions. Cambridge: Cambridge University Press, 1989.
39. Ruckenstein E, Prieve DC. Rate of deposition of Brownian particles under the action of London and double layer forces. *J Chem Soc Faraday Trans II*. 1973;69:1522–1536.
40. Kang NW, Lee S, Kim D, Hong S, Kweon JH. Analyses of calcium carbonate scale deposition on four RO membranes under a seawater desalination condition. *Water Sci Technol*. 2011;64:1573–1580.
41. Williams MMR, Loyalka SK. Aerosol Science, Theory and Practice. London: Pergamon Press, 1991.
42. Koutsou CP, Karabelas AJ. Shear stresses and mass transfer at the base of a stirred filtration cell and corresponding conditions in narrow channels with spacers. *J Membr Sci*. 2012;399–400:60–72.
43. Belfort G, Davis RH, Zydney AL. The behavior of suspensions and macro-molecular solutions in crossflow microfiltration. *J Membr Sci*. 1994;96:1–58.

Manuscript received Aug. 28, 2012, revision received Nov. 19, 2012, and final revision received Jan. 31, 2013.